Imaging and modeling of acute pressure-induced changes of collagen and elastin microarchitectures in pig and human resistance arteries

Bloksgaard, Maria ; Leurgans, Thomas; Spronck, Bart; Heusinkveld, Maarten Hg; Thorsted, Bjarne; Rosenstand, Kristoffer; Nissen, Inger; Hansen, Ulla Melchior; Brewer, Jonathan R.; Bagatolli, Luis; Rasmussen, Lars Melholt; Irmukhamedov, Akhmadjon ; Reesink, Koen D; De Mey, Jo G. R.

Published in:
American Journal of Physiology: Heart and Circulatory Physiology

DOI:
10.1152/ajpheart.00110.2017

Publication date:
2017

Document version
Publisher's PDF, also known as Version of record

Am J Physiol Heart Circ Physiol 313: H164–H178, 2017.
First published April 21, 2017; doi:10.1152/ajpheart.00110.2017.

RESEARCH ARTICLE | *Vascular Biology and Microcirculation*

Imaging and modeling of acute pressure-induced changes of collagen and elastin microarchitectures in pig and human resistance arteries

Maria Bloksgaard,[1] Thomas M. Leurgans,[1] Bart Spronck,[2] Maarten H. G. Heusinkveld,[2] Bjarne Thorsted,[3] Kristoffer Rosenstand,[1] Inger Nissen,[1] Ulla M. Hansen,[1] Jonathan R. Brewer,[3] Luis A. Bagatolli,[3] Lars M. Rasmussen,[4] Akhmadjon Irmukhamedov,[5] Koen D. Reesink,[2] and Jo G. R. De Mey[1,5]

[1]*Department of Cardiovascular and Renal Research, Institute of Molecular Medicine, University of Southern Denmark, Odense, Denmark;* [2]*Department of Biomedical Engineering, Cardiovascular Research Institute Maastricht, Maastricht University, Maastricht, The Netherlands;* [3]*MEMPHYS-Center for Biomembrane Physics, University of Southern Denmark, Odense, Denmark;* [4]*Department of Clinical Biochemistry and Pharmacology, Odense University Hospital, Odense, Denmark; and* [5]*Department of Cardiac, Thoracic and Vascular Surgery, Odense University Hospital, Odense, Denmark*

Submitted 15 February 2017; accepted in final form 14 April 2017

Bloksgaard M, Leurgans TM, Spronck B, Heusinkveld MHG, Thorsted B, Rosenstand K, Nissen I, Hansen UM, Brewer JR, Bagatolli LA, Rasmussen LM, Irmukhamedov A, Reesink KD, De Mey JGR. Imaging and modeling of acute pressure-induced changes of collagen and elastin microarchitectures in pig and human resistance arteries. *Am J Physiol Heart Circ Physiol* 313: H164–H178, 2017. First published April 21, 2017; doi:10.1152/ajpheart.00110.2017.— The impact of disease-related changes in the extracellular matrix (ECM) on the mechanical properties of human resistance arteries largely remains to be established. Resistance arteries from both pig and human parietal pericardium (PRA) display a different ECM microarchitecture compared with frequently used rodent mesenteric arteries. We hypothesized that the biaxial mechanics of PRA mirror pressure-induced changes in the ECM microarchitecture. This was tested using isolated pig PRA as a model system, integrating vital imaging, pressure myography, and mathematical modeling. Collagenase and elastase digestions were applied to evaluate the load-bearing roles of collagen and elastin, respectively. The incremental elastic modulus linearly related to the straightness of adventitial collagen fibers circumferentially and longitudinally (both $R^2 \geq 0.99$), whereas there was a nonlinear relationship to the internal elastic lamina elastin fiber branching angles. Mathematical modeling suggested a collagen recruitment strain (means ± SE) of 1.1 ± 0.2 circumferentially and 0.20 ± 0.01 longitudinally, corresponding to a pressure of ~40 mmHg, a finding supported by the vital imaging. The integrated method was tested on human PRA to confirm its validity. These showed limited circumferential distensibility and elongation and a collagen recruitment strain of 0.8 ± 0.1 circumferentially and 0.06 ± 0.02 longitudinally, reached at a distending pressure below 20 mmHg. This was confirmed by vital imaging showing negligible microarchitectural changes of elastin and collagen upon pressurization. In conclusion, we show here, for the first time in resistance arteries, a quantitative relationship between pressure-induced changes in the extracellular matrix and the arterial wall mechanics. The strength of the integrated methods invites for future detailed studies of microvascular pathologies.

NEW & NOTEWORTHY This is the first study to quantitatively relate pressure-induced microstructural changes in resistance arteries to the mechanics of their wall. Principal findings using a pig model system were confirmed in human arteries. The combined methods provide a strong tool for future hypothesis-driven studies of microvascular pathologies.

incremental elastic (Young's) modulus; extracellular matrix; two-photon excitation fluorescence microscopy; collagen recruitment

COLLAGEN, ELASTIN, AND GLYCOPROTEINS, the main constituents of the extracellular matrix (ECM), are major determinants of the mechanical properties of arteries. Detailed quantitative information on the relationship between the mechanics and the microarchitecture of the ECM in resistance arteries is lacking in human health and disease. Elastin dominates the compliant segment of the passive pressure-diameter curve at low distending pressures, whereas wall stress at higher pressures is increasingly borne by the more rigid collagen fibers (21, 32, 38, 66, 67). The spatial distribution of elastin is reported to define the biaxial wall mechanics in resistance arteries (17). Essential hypertension is associated with inward remodeling of the resistance arteries in humans as well as in experimental animal models (43, 47, 48, 64, 65). By sensing the circumferential wall stress on the ECM, smooth muscle cells (SMC) stimulate removal, rearrangement, and de novo synthesis of the ECM (38). In essential hypertension, remodeling of the arterial wall is associated with an increased collagen-to-elastin ratio and significantly increased wall stiffness (2, 40, 41). This is supported by studies in elastin-deficient mice (elastin$^{+/-}$) (68) and mice with a compromised elastin fiber integrity (fibulin-5$^{-/-}$), which both exhibit an increased stiffness of the arterial wall (8, 27). Not only the content and quality of elastin but also a local redistribution of elastin within the internal elastic lamina (IEL) is associated with an increased incremental elastic (Young's) modulus (E_{inc}) of the arterial wall and with the development of hypertension (12, 30). Cross-linking of collagen by transglutaminases (4, 5) further increases the stiffness of the arterial wall. A recent paper by Bell et al. (6) has opened discussion of the mechanobiology of vascular remodeling in human subcutaneous resistance arteries, reporting a reorganization of fibrous proteins upon increasing pressure.

Address for reprint requests and other correspondence: M. Bloksgaard, Dept. of Cardiovascular and Renal Research, Institute of Molecular Medicine, Univ. of Southern Denmark, J. B. Winsløws Vej 21, 3rd floor, 5000 Odense C, Denmark (e-mail: mbloksgaard@health.sdu.dk).

We have previously reported that the microarchitecture of elastin in human patient and pig pericardial resistance arteries (hPRA and pPRA, respectively) differs markedly from that of elastin in rat mesenteric arteries (rMA) (9), a frequently used animal model of essential hypertension. In rMA, the external elastic lamina (EEL) is a dense network of interconnected fibers, whereas the IEL has the structure of a sheet with holes (1, 12, 17, 30, 31, 53). In contrast, hPRA and pPRA lack a prominent EEL, and the IEL is composed of sparse longitudinally aligned elastin bundles interconnected by thinner elastin fibers. This structure of the IEL is similar to the one described for human subcutaneous resistance arteries (hSCAs) (6, 32). Finding a different microarchitecture of elastin in human resistance arteries raises questions on how the different microarchitecture of elastin is reflected in the arterial wall mechanics. This question is addressed in this work. We tested the hypothesis that the biaxial mechanics of resistance arteries mirror pressure-induced changes in the microarchitectures of collagen and elastin. We used pPRA for the initial development of methods for biomechanical testing, image acquisition, and data analyses. Furthermore, a mathematical model was applied to characterize the elastin and collagen components of the arterial wall with respect to intrinsic stiffness and to estimate the collagen recruitment strains (3, 66). Next, PRAs from patients with cardiovascular diseases were included to confirm the validity of the method, and future extensions and applications of the integrated approach are discussed.

MATERIALS AND METHODS

Ethical approval. Biopsies of the human parietal pericardium were collected after written informed consent, as previously described (9). The study of human tissues conformed with the principles outlined in the Declaration of Helsinki (70) and was approved by The Regional Committees on Health Research Ethics for Southern Denmark (S-20100044 and S-20140202) and the Danish Data Protection Agency.

Pig parietal pericardia were collected at a local abattoir. The collection and use of the pig tissue, regarded as waste, does not require ethical approval in Denmark.

Chemicals and reagents. Porcine pancreatic elastase (7.5 U/mg, catalog no. 324682, lot no. D00147595, Calbiochem, San Diego, CA) and phosphate buffered (pH 6.9) 4% formaldehyde solution (1.00496.9010) were from Merck Millipore (Hellerup, Denmark). Collagenase type 2 was from Worthington Biochemical (no. 4,174, 250 U/mg, batch 44C14824A, Lakewood, NJ). Endothelin-1 was obtained from Bachem (Weil am Rhein, Germany). 9,11-Dideoxy-9a,11a-methanoepoxy prostaglandin $F_{2\alpha}$ (U46619) was from Tocris Bioscience (Bristol, UK). All other chemicals were from Sigma-Aldrich (Brøndby, Denmark).

Biopsies. Human parietal pericardia were collected during coronary artery bypass grafting or valve replacement surgeries at the Odense University Hospital. Tissues were stored in sterile, ice-cold physiological salt solution [PSS; composed of (in mM) 115 NaCl, 25 $NaHCO_3$, 2.5 K_2HPO_4, 1.2 $MgSO_4$, 5.5 glucose, 10 HEPES, and 1.3 $CaCl_2$] at pH 7.4, as previously described (9). Resistance-sized arteries (±200 μm lumen diameter) were microdissected after overnight (16–20 h) storage at 4°C. Human PRA did not visibly recoil longitudinally upon excision from the pericardium ($n = 20$).

Domestic pig (*Sus scrofa domesticus*, Landrace/Yorkshire/Duroc strain) parietal pericardia were collected at a local abattoir. The storage and handling of pig tissue were identical to those of human tissue. Longitudinal recoiling of the arteries upon excision from the tissue was measured under a dissection microscope (branch to branch distance before and after excision).

Pressure myography. Arteries were dissected free of adipose tissue and mounted on glass capillaries (diameter: 60–70 μm) in a pressure myograph system (110P, Danish Myo Technology, Aarhus, Denmark). Arteries were equilibrated for 30 min at 37°C and minimal distending pressure (5 mmHg) before the first experiment. Pressure-diameter and length-longitudinal force measurements were registered under longitudinally isotonic conditions (zero axial force). Transmural pressure was subsequently increased to 100 mmHg in steps of 5–20 mmHg, with an inlet-outlet pressure gradient of 20 mmHg. Arteries were left to equilibrate for at least 5 min after each increase in pressure to ensure a stable diameter and longitudinal force. All experiments were conducted at 37°C. Arterial viability was tested before fixation, and only data from contractile arteries were included for analyses. All arteries were fixed at 100 mmHg in 4% formaldehyde at the end of the experiments and stored at 4°C until imaging for the determination of elastin/collagen volume densities.

Mechanical properties of pPRA were evaluated in normal PSS, as these arteries showed no signs of myogenic activity (constriction upon sudden or gradually increased pressure from 20 to 100 mmHg). Human PRAs were mounted in normal PSS and pressurized up to 20 mmHg, as described for pig PRAs. At 20 mmHg, PSS was exchanged by isotonic high-K^+ PSS (containing 20 mM NaCl and 95 mM KCl instead of 115 mM NaCl) to test for the ability of the artery to constrict in response to depolarization. Next, the subsequent pressure-diameter and length-longitudinal force measurements were conducted in Ca^{2+}-free PSS supplemented with 3 μM EGTA and 3 μM sodium nitroprusside (SNP) to avoid myogenic activity of these arteries.

Enzymatic treatment of pPRA at 20 and 70 mmHg was performed by exposing the arteries ablumenally, for 20 min, to either 1 U/ml elastase or 0.5 mg/ml collagenase in PSS. Use of higher concentrations of the enzymes resulted in either leakage or loss of contractility. After treatment at 20 mmHg, arteries were rinsed three times in Ca^{2+}-free PSS containing 3 μM SNP and 3 μM EGTA, and pressure was increased to 100 mmHg in steps of 20 mmHg, as described above.

Calculations of structural and mechanical parameters. Structural parameters were calculated as previously described (12, 13, 50). Wall thickness (WT; in μm) was calculated as follows:

$$\mathrm{WT} = 0.5\varnothing_{\mathrm{out}} - 0.5\varnothing_{\mathrm{in}} \quad (1)$$

where $\varnothing_{\mathrm{out}}$ and $\varnothing_{\mathrm{in}}$ are the outer and inner diameters of the artery, respectively. Wall cross-sectional area ($\mathrm{CSA_{wall}}$; in μm^2) was calculated as follows:

$$\mathrm{CSA_{wall}} = \frac{\pi(\varnothing_{\mathrm{out}}^2 - \varnothing_{\mathrm{in}}^2)}{4} \quad (2)$$

The wall thickness-to-lumen diameter ratio (*W/L*) was calculated as follows:

$$W/L = \frac{2\mathrm{WT}}{\varnothing_{\mathrm{in}}} \quad (3)$$

Calculations of stresses, strains, and other mechanical properties were performed as previously described (34, 55) under the thin wall assumption.

Circumferential properties [circumferential stretch ratio (λ_θ), circumferential strain (ε_θ), and circumferential stress (σ_θ; in Pa)] were defined and calculated as follows:

$$\lambda_\theta = \frac{\varnothing_{\mathrm{in}}}{\varnothing_{\mathrm{in,0\ mmHg}}} \quad (4)$$

$$\varepsilon_\theta = \frac{\varnothing_{\mathrm{in}} - \varnothing_{\mathrm{in,0\ mmHg}}}{\varnothing_{\mathrm{in,0\ mmHg}}} \quad (5)$$

$$\sigma_\theta = \frac{\mathrm{P}\varnothing_{\mathrm{in}}}{2\mathrm{WT}} \quad (6)$$

where P is pressure.

Longitudinal properties [longitudinal stretch ratio (λ_z), longitudinal strain (ε_z), longitudinal stress (σ_z; in Pa), and longitudinal force (F_z; in N)] were defined and calculated as follows:

$$\lambda_z = \frac{L}{L_0} \tag{7}$$

$$\varepsilon_z = \frac{L - L_0}{L_0} \tag{8}$$

$$\sigma_z = \frac{F_z}{\mathrm{CSA}_{\mathrm{wall}}} \tag{9}$$

$$F_z = \frac{P\pi\varnothing_{\mathrm{in}}^2}{4} + F_{(z,\mathrm{red})} \tag{10}$$

where L is length.

F_z in this study simplifies to

$$F_z = \frac{P\pi\varnothing_{\mathrm{in}}^2}{4} \tag{11}$$

as reduced axial force ($F_{z,\mathrm{red}}$) was maintained at 0.

Mathematical modeling and calculations. Incremental elastic moduli were determined circumferentially, as well as longitudinally. Generally, the incremental elastic modulus (E_{inc}; in Pa) was calculated as follows:

$$E_{\mathrm{inc}} = \frac{d\sigma}{d\varepsilon} = \sigma_0\beta e^{\beta\varepsilon} = \beta\sigma \tag{12}$$

and thus

$$E_{\mathrm{inc},\theta} = \sigma_\theta\beta_\theta \tag{13}$$

and

$$E_{\mathrm{inc},z} = \sigma_z\beta_z \tag{14}$$

β-values were estimated by fitting the following single-exponential equation to the measured stress-strain relationship:

$$\sigma = \sigma_0 e^{\beta\varepsilon} \tag{15}$$

The goodness of fit was evaluated by looking at the residuals plot along with the R^2 of the fit. β-Values were included for the calculation of E_{inc} for fits with $R^2 > 0.7$ and randomly distributed residuals.

Circumferential stress-strain data for hPRA and pPRA (only those not treated with elastase or collagenase) were fitted with the following three-parameter mathematical model according to Ref. 3:

$$\sigma = E_{\mathrm{elastin}} \times \varepsilon + E_{\mathrm{collagen}} \times \max\left(\varepsilon - \varepsilon_{\mathrm{ho}}, 0\right) \tag{16}$$

This method was used to estimate the elasticity of elastin and collagen in the arterial wall and to estimate the strain ($\varepsilon_{\mathrm{ho}}$) at which collagen is engaged ["hook on" (66)]. Errors between measured wall stress and model-predicted wall stress were quantified by the normalized root mean square error (NRMSE), as given by:

$$\mathrm{NRMSE} = \frac{1}{\overline{\sigma}_{\theta,\mathrm{meas}}}\sqrt{\frac{1}{N}\sum_{i=1}^{N}\left(\sigma_{\theta,\mathrm{meas},i} - \sigma_{\theta,\mathrm{Bakker},i}\right)^2} \times 100\% \tag{17}$$

where $\overline{\sigma}_{\theta,\mathrm{meas}}$ is equal to the average measured circumferential wall stress and $\sigma_{\theta,\mathrm{meas},i}$ and $\sigma_{\theta,\mathrm{Bakker},i}$ are the measured wall stress and model-predicted wall stress, respectively, resulting from fitting the mathematical function, as previously described (3). N is the number of data points.

Two-photon excitation fluorescence microscopy of isolated vital arteries for the determination of IEL branching angles and collagen straightness. Arteries were dissected free of periarterial adipose tissue and mounted on capillaries (diameter: 60–70 μm) in a custom-built pressure myograph (subject to DK patent no. 201200167, University of Southern Denmark, J. Schoubo, V. Jensen, F. Jensen, and T. R. Uhrenholt) designed for vital imaging using a custom-built two-photon excitation fluorescence microscopy setup on a Nikon TI Eclipse platform (10). The objective was a ×60 water immersion objective (numerical aperture: 1.29). Excitation light was 820 nm (HPeMaiTai DeepSee, Spectra Physics, Mountain View, CA). Emission was split by a ChromaET 460 nm long-pass dichroic and collected in two channels at 520/35 and 402/15 nm (Semrock FF01-520/35-25 BrightLine filter and Chroma ET402/15× band-pass filter, respectively) using Hamamatsu H7422P-40 PMTs (Ballerup, Denmark). Dichroic and band-pass filters were from AHF analysentechnik AG (Tübingen, Germany).

Imaging experiments were conducted in HEPES-buffered PSS (36) [composed of (in mM) 144 NaCl, 4.7 KCl, 2.5 $CaCl_2$, 1.2 $MgSO_4$, 1.2 KH_2PO_4, 14.9 HEPES, and 5.5 glucose] adjusted to pH 7.4 with NaOH at 37°C. Arteries were equilibrated at a transmural pressure of 20 mmHg for 30 min before any imaging was conducted. Pressurization was performed under longitudinally isotonic conditions (zero axial force) by adjusting the length of the artery, according to the changes in longitudinal force. After equilibration at 20 mmHg, pressure was increased gradually in steps of 20 mmHg to 100 mmHg. Equilibration for at least 10 min at each step was allowed before z-imaging stacks were obtained.

Branching angles of the elastin fibers in the IEL were measured by manual markup on maximum intensity projections of two to seven consecutive images from z-image stacks of the IEL using the angle tool in FIJI (56). Seven to 30 angles were measured for each sample and each pressure step, with an average number of observations of 13/18/21 (pPRA) and 13/10/14 (hPRA) at 20/40/100 mmHg, respectively.

Collagen straightness was determined using the FIJI NeuronJ plugin (46), as previously described by Rezakhaniha and Agianniotis (51). Individual images of the adventitial collagen in close proximity to the external elastic lamina/tunica media were analyzed. A ratio of L_0/L_f [collagen fiber bundle end-to-end length via a straight line (L_0)/full length (L_f)] close to 1 indicates an almost straight collagen fiber. Five to 26 individual fibers were analyzed for each sample at each pressure step, with an average number of observations 16/15/12 (pPRA) and 9/10/16 (hPRA) at 20/40/100 mmHg, respectively.

Two-photon excitation fluorescence microscopy of fixed arteries and ilastik image analyses of elastin/collagen volume densities. Collagen and elastin volume densities were determined in two or three image stacks per isolated pressure-fixed artery (n = 8 pPRAs and n = 9 hPRAs). Only arteries not exposed to collagenase or elastase were included. Imaging was performed using an Olympus FluoView 1000 microscope equipped with a XLPLN ×25 W (numerical aperture: 1.05) objective lens. Excitation light (MaiTai, Spectra Physics, Mountain View, CA) was 820 nm for elastin and 990 nm for collagen (to avoid any excitation of elastin and other autofluorescent proteins). Emission was split between detectors using a DM505 dichroic mirror. Collagen second harmonic generation was picked up at 495 nm using a BA420-500 filter, and elastin autofluorescence was picked up using a BA495-540HQ filter. Image stacks were acquired at 1,024 × 1,024 pixel density with 1 μm/section in z, with the field of view spanning the width of the individual artery. Image data were analyzed using ilastik software (61). TIFF image stacks were first converted to HDF5 format using FIJI (56), and quantitative data processing of results from ilastik was performed using MatLab (R2015b, MathWorks, Natick, MA). Data on elastin and collagen were analyzed separately in ilastik. The results were for all image stacks verified by visual comparison between the final image masks and the raw image files. For a few image stacks with unsatisfactory results, the ilastik masks were optimized, and the images were reanalyzed. Intra-assay (within artery) variability was 25% and 21% for pPRA and hPRA, respectively.

Statistics. All data are presented as means ± SE with the number of observations (n) indicated. Where applicable, dot plots are used for clarity. Statistical analyses were conducted using GraphPad Prism for Windows (version 6.05). We aimed at adhering to the advisory guidelines on statistical reporting recently emphasized by the *Journal of Physiology* and other journals (22–26). All tests were performed for the null hypothesis (H_0), stating that the given treatment or change in conditions was inducing no effect, and the alternative hypothesis (H_A, to be accepted in case the null hypothesis is rejected) stating that the treatment effect or change is significant, with the predicted direction of change included for one-tailed tests. The GraphPad Prism inbuilt D'Agostino and Pearson omnibus normality test was included for sample sizes ≥ 20 and when $P < 0.05$, data were $\log_{10}$ transformed, and normal distribution was then met. For statistical analyses, where sample sizes were smaller than 20, normality was assumed as was an equal variance between samples to be compared. P values are reported as calculated, with the difference between means immediately after, followed by the computed 95% confidence interval (CI) for the difference between the group means. The level of significance was 0.05. Pressure-dependent changes in the microarchitecture of collagen and elastin (Fig. 3, *A* and *B*) were analyzed using repeated-measures one-way ANOVA with the Greenhouse-Geisser correction for violation of sphericity (as sphericity was not assumed). The relationship between E_{inc} and collagen straightness or IEL elastin fiber branching angles (Fig. 3, *C* and *D*) was assessed by fitting the plotted data with a linear regression. The data shown in Figs. 4 and 7 were analyzed using a paired t-test (θ vs. z) under the assumption of normal distribution. The effect of enzymatic treatment (Fig. 5) on diameter and wall thickness was tested using paired two-tailed t-tests. One-tailed t-tests were used for evaluating the impact on length of the enzymatic treatments (H_0: $L_{after} - L_{before} \leq 0$ and H_A: $L_{after} - L_{before} > 0$) and, for comparison, between the enzymatic treatments (H_0: $value_{collagenase} - value_{elastase} \leq 0$ and H_A: $value_{collagenase} - value_{elastase} > 0$). The effect of enzymatic treatment at 20 mmHg on the circumferential and longitudinal stretches during pressurization to 100 mmHg (Fig. 6, *A* and *B*) was analyzed by repeated-measures two-way ANOVA followed by Dunnett's multiple-comparison test with main treatment (enzyme) effect for data obtained after enzymatic treatment only (i.e., 20–100 mmHg). Statistical analyses of the hPRA collagen straightness and IEL branching angles (Fig. 10) were performed using one-way ANOVA.

RESULTS

Biaxial mechanics of pPRA. pPRA were used for the development of protocols and methods and for initial testing of the hypothesis. Pigs were a mixture of ~7-mo-old castrated males and females, and the PRA from these were used to establish the relationship between the microarchitecture and mechanics of the PRA and to evaluate the load-bearing roles of collagen and elastin. Longitudinal recoil of the pPRA averaged 21 ± 1% (n = 31) upon excision from the parietal pericardium, reflecting an in vivo axial stretch ratio of $\lambda_z = 1.27 \pm 0.1$. Upon pressurization to 100 mmHg, the internal diameter of the pPRA (n = 20) approximately doubled to reach an internal diameter at 100 mmHg of 217 ± 17 μm, whereas length increased by 35 ± 5% (Fig. 1). Wall thickness decreased from 51 ± 4 to 31 ± 2 μm and the resulting wall-to-lumen ratio at 100 mmHg was 29 ± 1%. Circumferential (hereafter noted by subscript "θ") wall stress reached 47 ± 2 kPa, whereas longitudinal

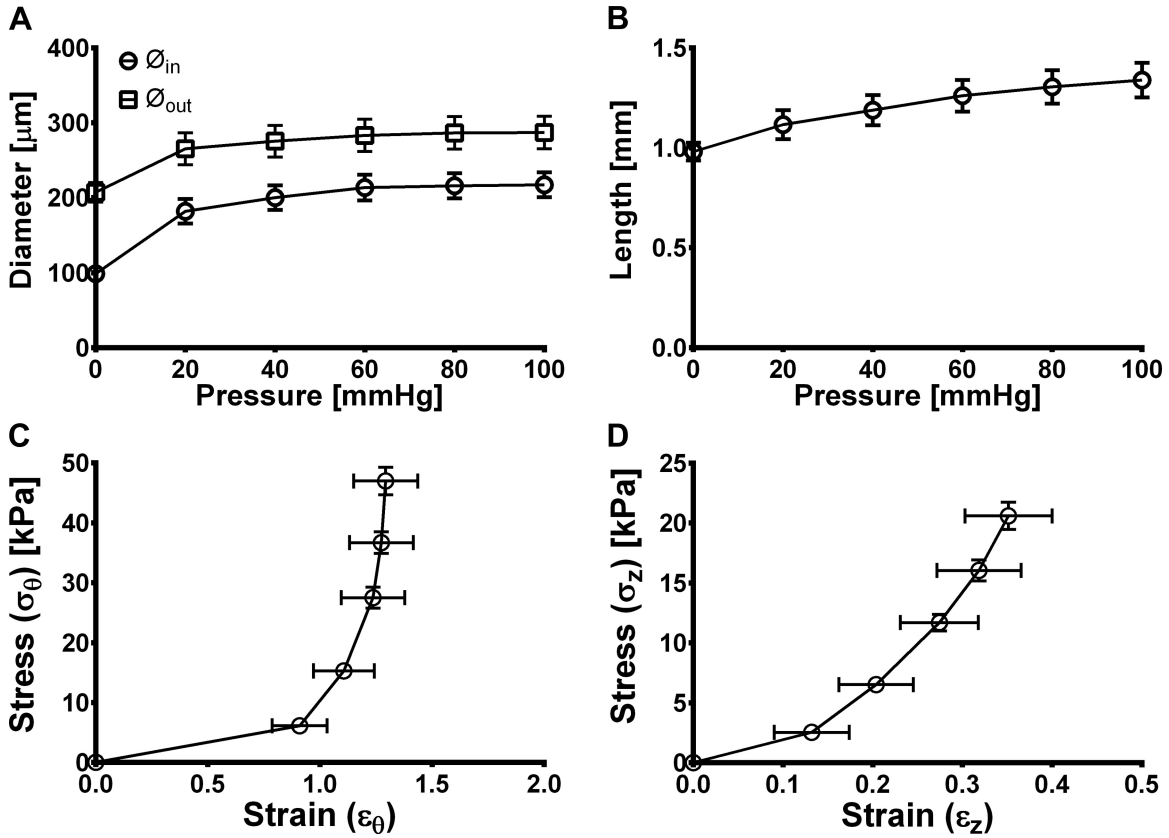

Fig. 1. Structural and mechanical characteristics of pig pericardial resistance arteries (pPRAs) as a function of increasing transmural pressure. *A*: pressure-diameter, *B*: pressure-length, *C*: circumferential stress (σ_θ)-strain (ε_θ) and *D*: longitudinal stress (σ_z)-strain (ε_z) relationships from 20 individual pPRAs. $Ø_{out}$ and $Ø_{in}$ are the outer and inner diameters of the artery.

(hereafter noted by subscript "z") stress, on average, reached 21 ± 1 kPa. Incremental elastic (Young's) moduli [E_{inc}, i.e., geometry-independent measures of wall stiffness (21)] were determined by first fitting the stress-strain relationships of the individual arteries to the single-exponential function $\sigma = \sigma_0 e^{\beta\varepsilon}$ (least-squares method, R^2_θ: 0.95 ± 0.01 (20) and range$_\theta$: 0.78–1.0; R^2_z: 0.97 ± 0.004 (20) and range$_z$: 0.90–0.99), as previously described (21, 31), followed by the calculation of $E_{inc} = \sigma\beta$ at the different distending pressures. By this method, mean $E_{inc,\theta}$ and $E_{inc,z}$ at 100 mmHg were 283 ± 32 kPa (range: 99–580) and 313 ± 99 kPa (median: 162.9 and range: 85–2,139), respectively (dot plots of individual β-values and E_{inc} are shown in Fig. 4).

Microarchitecture of the ECM is reflected in arterial wall mechanics. The microarchitecture of the ECM in pPRA was approached by the branching angles of the elastin fibers in the IEL and by the straightness of adventitial collagen fibers (51). Representative images of a pPRA are shown in Fig. 2. The "baseline" microarchitecture of the arteries was determined at 20 mmHg (Fig. 2, *A–D*), and additional measurements were performed at transmural pressures of 40 mmHg (Fig. 2, *E–H*) and 100 mmHg (Fig. 2, *I–L*). Quantitative measures of the straightness of adventitial collagen and the IEL elastin fiber branching angles are shown in Fig. 3, *A* and *B*, respectively. The straightness of the adventitial collagen bundles, determined for 6 pPRAs that were subjected to vital imaging, was positively and linearly related to both the circumferential and longitudinal incremental elastic modulus of the arterial wall of 20 other pPRAs subjected to pressure myography ($R^2_\theta = 0.99$ and $y = 1{,}750x - 1{,}389$; $R^2_z = 0.99$ and $y = 1{,}934x - 1{,}533$; Fig. 3*C*). The IEL branching angles showed a nonlinear relationship with the incremental elastic moduli, where both changed more dramatically between 20 and 40 mmHg compared with the changes between 40 and 100 mmHg (Fig. 3*D*).

Mathematical modeling of biomechanical data for the estimation of collagen and elastin stiffness and collagen recruitment strain. To assess the stiffness of the elastin and collagen components of the arterial wall, we applied a mathematical model (3, 66). This relatively simple model allows extraction of three important measures: the stiffness of collagen, the stiffness of elastin, and the collagen recruitment strain, i.e., the strain of the arterial wall, where collagen fibers start to limit further expansion of the artery with increasing pressure. These three parameters are important for future comparative studies, e.g., between hypertensive and normotensive patients, or in studies of hypertensive animal models. Important for the interpretation of the model estimates, especially when comparing subgroups, is the establishment of the elastin/collagen volume density by three-dimensional imaging of the entire thickness of the vascular wall. In pPRA, this was 40 ± 7% (n = 8), with a 95% CI of 31–64% (Fig. 4*D*). The findings from the mathematical modeling are shown in Fig. 4. The three-parameter

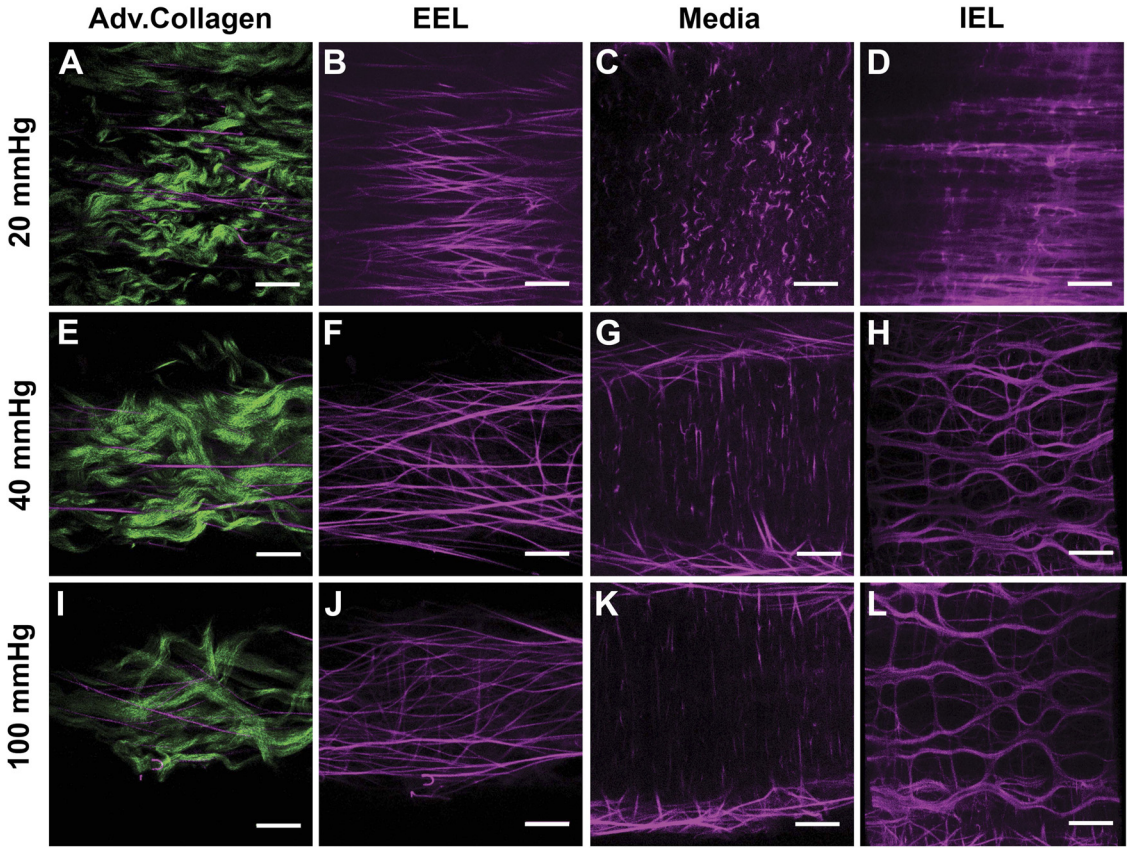

Fig. 2. Microarchitecture of the extracellular matrix of pPRAs as a function of increasing transmural pressure. Two-photon excitation fluorescence microscopy images of collagen (green) and elastin (magenta) at 20 mmHg (*A–D*), 40 mmHg (*E–H*), and 100 mmHg (*I–L*) in the tunica adventitia (*A*, *E*, and *I*), external elastic lamina (EEL; *B*, *F*, and *J*), tunica media (*C*, *G*, and *K*), and internal elastic lamina (IEL; *D*, *H*, and *L*) are shown. The image series is representative of six independent experiments. Scale bars = 10 μm.

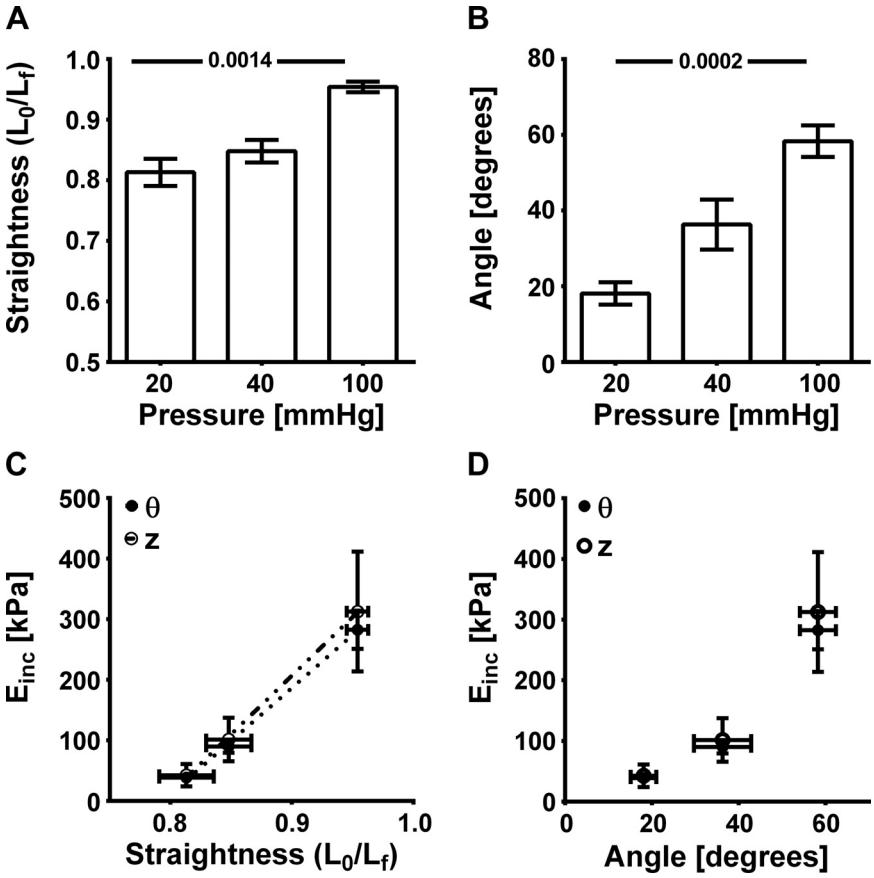

Fig. 3. Microstructural changes in adventitial collagen and the IEL in relation to the circumferential and longitudinal incremental elastic moduli (E_{inc}). *A*: straightness L_0/L_f [collagen fiber bundle end-to-end length via a straight line (L_0)/full length (L_f)] of collagen fibers present at the border between the EEL and tunica adventitia. *B*: branching angles for elastin fibers in the IEL determined for six individual arteries. *P* values and corresponding *F* values were determined using repeated-measures one-way ANOVA [*P*/*F* values: 0.0014/24.18 (*A*) and 0.0002/37.38 (*B*)]. *C*: mean collagen straightness, determined for six pPRAs subjected to vital imaging, correlated linearly with mean E_{inc} calculated for 20 other pPRAs subjected to pressure myography, both circumferentially ($R^2 = 0.99$, $y = 1{,}750x - 1{,}389$) and longitudinally ($R^2 = 0.99$, $y = 1{,}934x - 1{,}533$). *D*: mean IEL branching angles of the six pPRAs correlated nonlinearly with mean E_{inc} calculated for the 20 other pPRAs subjected to pressure myography.

mathematical modeling of the pPRA circumferential stress-strain relationships showed, as expected, a significantly lower elastic modulus of the elastin part of the wall ($E_{elastin,\theta}$) compared with the collagen part of the wall [$E_{collagen,\theta}$, difference between means $E_{collagen,\theta} - E_{elastin,\theta} = \log 1.176$ (0.96–1.39), $P < 0.0001$]. Likewise, longitudinally, the elastic modulus of collagen ($E_{collagen,z}$) in pPRAs was significantly higher compared with $E_{elastin,\theta}$ [difference of log 0.52 (0.32–0.73), $P < 0.0001$]. The longitudinal stress-strain relationships differed from those of the circumference. The pPRA showed markedly higher strains circumferentially than longitudinally [difference in strain at 100 mmHg ($\theta - z$): 0.9 (0.6−1.3), $P < 0.0001$; Fig. 1, *C* and *D*]. When data on $E_{elastin}$ and $E_{collagen}$ for the circumference were compared with data for the longitudinal direction (Fig. 4*E*), the values for $E_{elastin,z}$ were higher compared with $E_{elastin,\theta}$ [log mean difference: 0.44 (0.23–0.65), $P < 0.0001$ by two-tailed *t*-test]. Neither the data nor a statistical analysis provided conclusive evidence for a difference between $E_{collagen,\theta}$ and $E_{collagen,z}$ [mean difference: 0.21 (0.0–0.42), $P = 0.061$] despite a tendency toward $E_{collagen,z}$ being lower compared with $E_{collagen,\theta}$. The final parameter obtained from the three-parameter mathematical modeling was an estimate of the strain where collagen is engaged ["hook-on strain" (66)]. For the pPRA, collagen was engaged circumferentially at a significantly higher strain (1.1 ± 0.2) than longitudinally [0.2 ± 0.01, mean difference: 0.87 (0.5–1.2), $P < 0.0001$; Fig. 4*F*]. It should be noted that the NRMSE, the error between measured wall stress and model-predicted wall stress, showed a higher variability circumferentially than longitudinally (Fig. 4*G*).

Elastin plays a prominent role in bearing longitudinal stress. Elastase and collagenase were applied ablumenally for 20 min on pressurized pPRA to evaluate the load-bearing roles of elastin and collagen, respectively. Both treatments, at 70 mmHg, resulted in significant lengthening of the pPRA ($\Delta L_{elastase} = 8 \pm 2\%$, $P = 0.0026$, and $\Delta L_{collagenase} = 13 \pm 3\%$, $P = 0.0005$), whereas arterial diameter and wall thickness remained unchanged (Fig. 5, *C* and *D*). Similar observations were made after enzymatic treatment at 20 mmHg, at which both elastase and collagenase treatment increased the length of the pPRA significantly ($\Delta L_{elastase} = 20 \pm 4\%$, $P = 0.0007$, and $\Delta L_{collagenase} = 6 \pm 2\%$, $P = 0.0021$; Fig. 5, *A* and *B*). Elastase treatment at 20 mmHg increased the length of the treated arteries to a larger extent than collagenase treatment [difference: 14% (4–24%), $P = 0.0043$], whereas the enzyme-induced changes in length at 70 mmHg were not different between treatments ($P = 0.10$). Collagenase treatment at 20 mmHg, furthermore, induced a significant permanent increase in the arterial lumen diameter ($\Delta \varnothing_{in} = 14 \pm 4\%$, $P = 0.004$). Consequently, after collagenase treatment at 20 mmHg, the pressure-diameter curve shifted significantly upward over the entire pressure range of 20–100 mmHg (Fig. 6*A*), whereas elastase and, to a lesser extent, collagenase treatment induced an upward shift of the pressure-length curve (Fig. 6*B*). As shown in the stress-strain curves for the enzyme-treated arteries (Fig. 6, *C* and *D*), elastase treatment shifted the circumferential stress-strain curve leftward, whereas collagenase treatment shifted the circumferential stress-strain curve rightward. Longitudinally, elastase shifted the stress-strain curve rightward, whereas collagenase treatment, rather than changing the

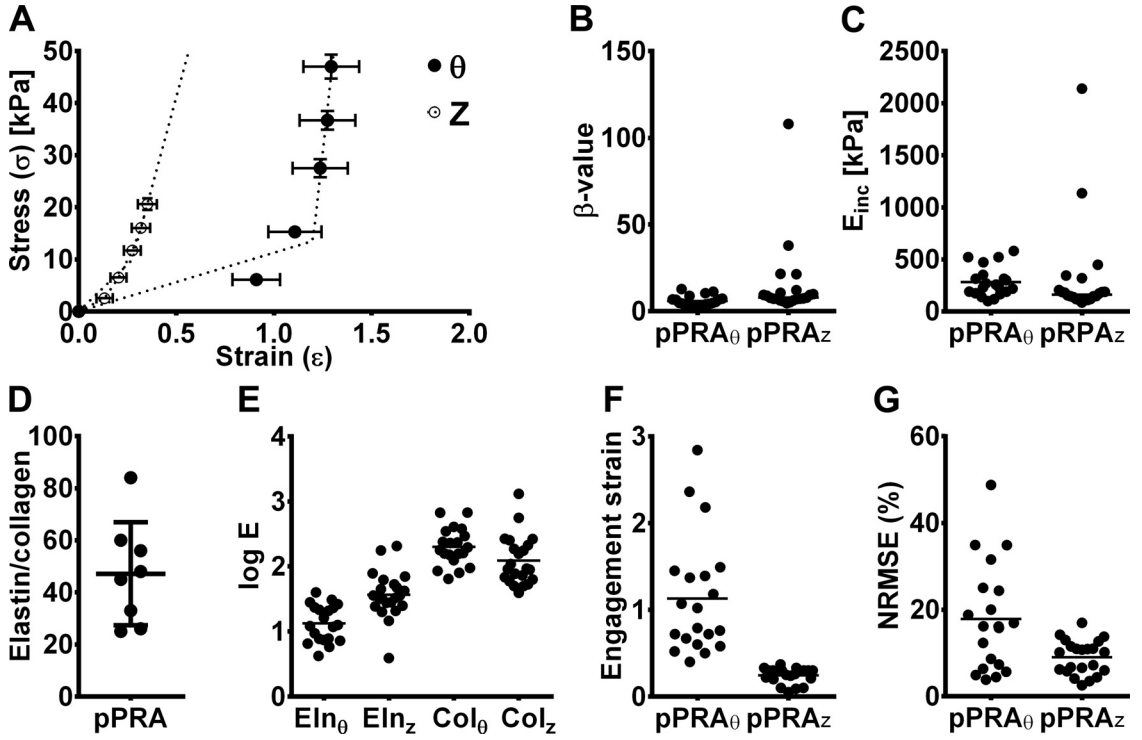

Fig. 4. Parameter estimates from fitting the stress-strain relationships and mathematical modeling of the pPRA. *A*: stress-strain relationship with the mathematical model (dotted lines) superimposed on the original data points [circumference (θ): ●; longitude (*z*): ○]. *B*: individual β-values. *C*: calculated E_{inc} at a transmural pressure of 100 mmHg. *D*: elastin-to-collagen volume ratios were calculated from imaging data. *E*: elastin (Eln) and collagen (Col) stiffness in the circumferential and longitudinal directions, respectively. *F*: collagen recruitment strain, estimated from the mathematical model. *G*: normalized root mean square error (NRMSE), a measure of the errors between measured wall stress and model-predicted wall stress.

shape of the curve, extended it toward higher strains and stresses. Curve fitting and mathematical modeling of the stress-strain relationships of arteries treated with the enzymes at 20 mmHg were not performed due to the discontinuity in the data (enzyme treatments were performed at 20 mmHg, i.e., data at 0–20 mmHg are for untreated arteries, whereas data points at 20–100 mmHg are for enzyme-treated arteries). Arteries exposed to elastase or collagenase remained responsive to a vasoconstrictor; however, endothelium-dependent vasodilation in response to 1 μM bradykinin was impaired, in particular, for collagenase-treated arteries (data not shown). Imaging during enzyme digestions suggested qualitative rather than quantitative changes upon the enzyme treatments. Elastin fibers were still found after elastase treatement when the imaging conditions were optimized and spot-wise larger, longitudinally aligned disruptions were observed in collagen post collagenase treatment rather than with general removal of the matrix. An effect of the elastase on other components of the ECM cannot be excluded, as collagen, normally not showing autofluorescence, showed autofluorescence after elastase digestion (data not shown).

hPRAs display limited elongation upon pressurization to 100 mmHg. hPRAs were included in the study to confirm the validity of the integrated methodological approach. hPRAs were obtained from patients with cardiovascular diseases, an interesting group for future detailed studies of human resistance artery mechanobiology in diseased states. Patients were recruited before coronary artery bypass grafting and valve replacement surgeries. They were, on average, 64 ± 2-yr-old (range: 50–80) men ($n = 7$) and women (n = 5). Ten of the twelve patients received antihypertensive medication (for one patient, information was not available; another patient was not diagnosed with hypertension). Upon pressurization to 100 mmHg, the mean diameter of hPRA increased from 102 ± 13 to 184 ± 16 μm (Fig. 7). Wall thickness decreased from 50 ± 4 to 30 ± 2 μm and the corresponding wall-to-lumen ratio at 100 mmHg was 17.8 ± 2.4%. Interestingly, 6 of 12 hPRA showed no change in length upon pressurization to 100 mmHg, and the remaining 6 hPRAs showed limited length changes only (9.6 ± 2%), resulting in an average longitudinal strain at 100 mmHg of only 0.05 ± 0.02 (Fig. 7*D*), in agreement with no measureable recoiling of the hPRA upon excision from the tissue. Circumferential and longitudinal wall stress at 100 mmHg were 43 ± 4 and 19 ± 2 kPa, respectively (Fig. 7, *C* and *D*). Exponential fitting of the stress-strain relationships to determine the geometry-independent measure of wall stiffness, the β-value (Fig. 8*B*, proportional to E_{inc}, Fig. 8*C*), was performed for all 12 hPRA circumferentially, but only data from 6 of 12 hPRA showed a biphasic stress-strain relationship longitudinally. The goodness of the exponential fits was R^2_θ: 0.93 ± 0.02 and range$_\theta$: 0.80–1.00 and R^2_z: 0.83 ± 0.03 ($n = 6$) and range$_z$: 0.73–0.93. As a consequence, E_{inc} at 100 mmHg can only be calculated for the longitudinal component of the arterial wall for these six individuals. Because of the low number of observations and the large degree of variability between group variances, statistical analyses must be interpreted with caution. Under the assumption of normal distribution, paired *t*-testing (θ vs. *z*) supported that the hPRA shows a significantly higher β-value longitudinally (mean difference:

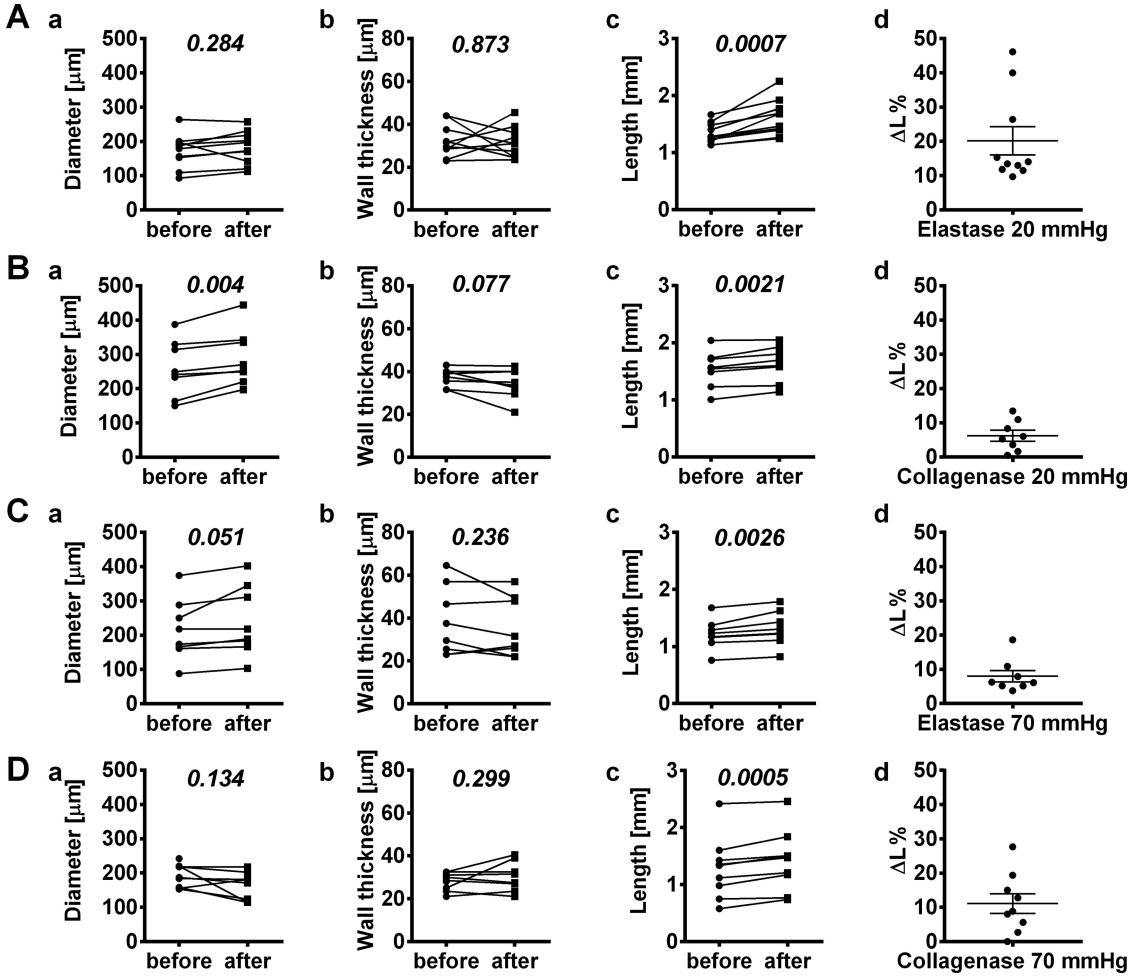

Fig. 5. Effects of elastase and collagenase treatment on diameter, wall thickness, and length of pPRAs. *A*: effect of elastase treatment at 20 mmHg, *B*: collagenase treatment at 20 mmHg, *C*: elastase treatment at 70 mmHg, and *D*: collagenase treatment at 70 mmHg on the diameter (*a*), wall thickness (*b*), and length (*c*), respectively, and the accompanying length increase as a percentage (*d*). Paired two-tailed *t*-tests were used for analyses with the exception that tests for increases in length upon enzymatic treatments were one-tailed.

64 ± 40, $P = 0.023$), whereas the obtained data did not support a statistically significant difference in E_{inc} at 100 mmHg ($P = 0.095$). hPRA $E_{inc,\theta}$ and $E_{inc,z}$ were 436 ± 76 kPa (10) and 996 ± 243 kPa (6), respectively.

Mathematical modeling shows that collagen is recruited at low strain in hPRAs. Similarly, as done for the pPRA, we applied a mathematical model to estimate the stiffness of collagen and elastin in the arterial wall and determined whether our prediction on the basis of the above observations of a very low collagen recruitment strain could be confirmed (Fig. 8*A*). Imaging was also performed of the segments from the pressure myograph to determine the elastin/collagen volume density in the arterial wall. The elastin-to-collagen ratio was 40 ± 20% (95% CI: 25–56; Fig. 8*D*). Circumferentially, the hPRA showed, like the pPRA, that $E_{elastin,\theta}$ was significantly smaller than $E_{collagen,\theta}$ [log mean difference: 1.59 (1.28–1.89), $P < 0.0001$; Fig. 8*E*]. As described above, six of the hPRA did not change axial geometry at all and, as such, did not fulfill the prerequisites for the three-parameter fitting method. The remaining six hPRAs did fulfill the requirements for fitting, although the results were highly variable between the individual hPRAs (Fig. 8, *E*–*G*). The variation in the data for $E_{elastin,z}$ was large, whereas the data for $E_{collagen,z}$ showed a smaller variability. Taking this into account, the data indicated that $E_{collagen,z}$ is higher compared with $E_{elastin,z}$, but, because of the low number of observations and the large degree of variability between group variances, statistical testing was not performed. It can be immediately seen in Fig. 8*E* that the estimated stiffness for collagen circumferentially and longitudinally showed little within-group variability when compared, and $E_{collagen,\theta}$ was significantly smaller compared with $E_{collagen,z}$ (log mean difference: −0.21 ± 0.04, $P = 0.006$). Collagen engagement strain for the hPRA was also significantly larger circumferentially (0.78 ± 0.08) than longitudinally (0.06 ± 0.02, mean difference: 0.77 ± 0.09, $P = 0.0004$; Fig. 8*F*). It is important to note that the NRMSE showed quite some variability between the individual hPRA samples (Fig. 8*G*), especially longitudinally.

Vital imaging confirms collagen recruitment at low strains in hPRAs. The above findings led us to investigate whether there was a lack of microarchitectural changes in the ECM of hPRAs in response to increasing pressure. The microarchitecture of both elastin and collagen fibers in the hPRA, visualized using vital imaging, did not noticeably change during pressur-

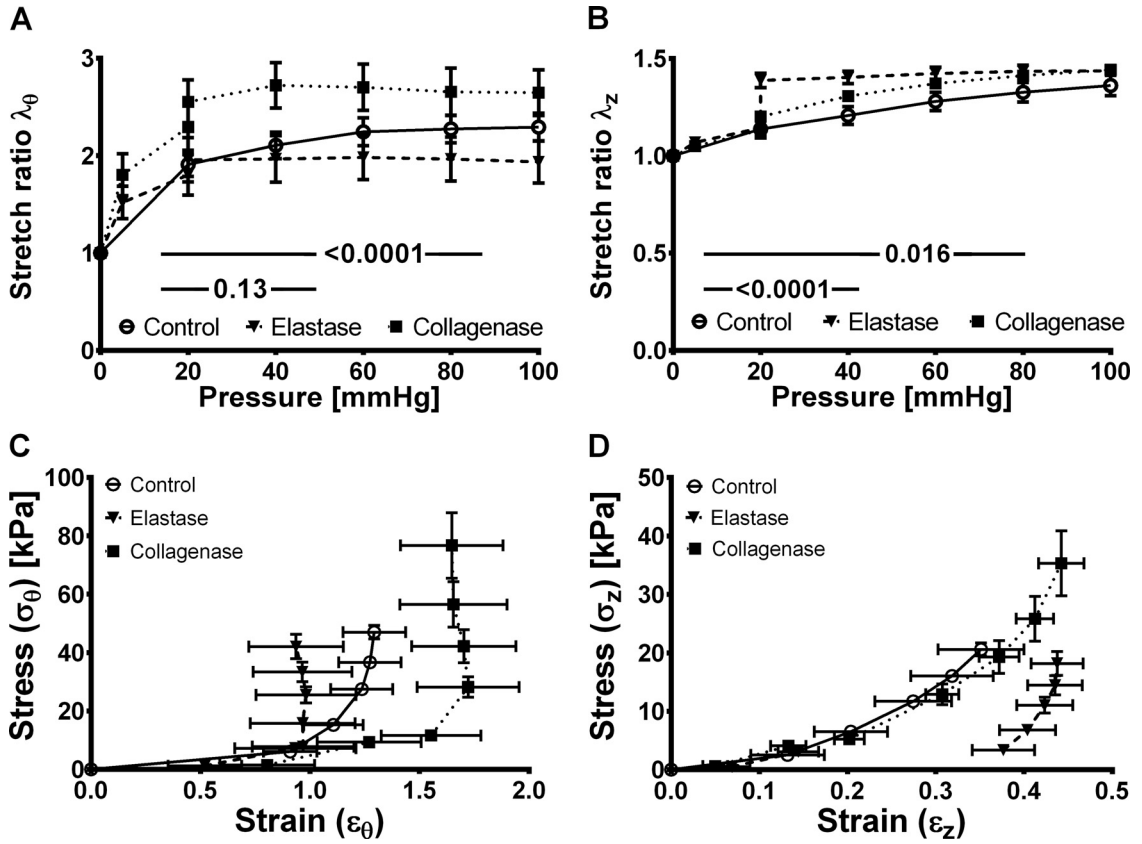

Fig. 6. Effect of elastase and collagenase treatment at 20 mmHg on the structural and mechanical properties of pPRAs as a function of increasing pressure. *A*: pressure-diameter stretch ratio. *B*: pressure-length stretch ratio. *C*: circumferential stress-strain relationships. *D*: longitudinal stress-strain relationships. Adjusted *P* values (*A* and *B*) were determined by repeated-measures two-way ANOVA followed by Dunnett's multiple-comparisons test with main treatment (enzyme) effect for data obtained.

ization from 20 to 100 mmHg (Fig. 9). The majority of collagen fibers were straight already at a pressure of 20 mmHg (Fig. 9, *A* and *B*), and elastin fibers of the IEL remained parallel during pressurization (Fig. 9, *D*, *H*, *L*), supporting the above observations of the hPRA being highly limited geometrically due to the microarchitecture and mechanical properties of the ECM. Quantitative analyses underlined the observations that collagen is straight at low pressures and that the structural changes in the IEL with increasing pressure are limited (Fig. 10). Compared with the pPRA, which showed a collagen straightness of ~0.8 at 20 mmHg, hPRA collagen straightness was >0.95 already at 20 mmHg, and IEL branching angles were at maximum ~30° at 100 mmHg, whereas pPRA IEL angles reached 60° at 100 mmHg.

DISCUSSION

With pressure myography and vital imaging, we confirmed the hypothesis that the vascular wall mechanics mirror the pressure-induced changes in the microarchitecture of collagen and elastin in PRAs. pPRAs were used for initial testing of the hypothesis and for testing the load-bearing roles of collagen and elastin. In these arteries, pressure induces an increase in the straightness of the adventitial collagen fibers linearly related to the circumferential as well as longitudinal incremental elastic moduli. In contrast, there is a nonlinear relationship of the incremental elastic modulus, both radially and axially, to the pressure-induced increase in the IEL elastin fiber branching angles.

Next, we applied the integrated method to hPRAs isolated from patients with cardiovascular diseases. hPRAs showed little pressure-induced radial distension and elongation but reached similar diameters at 100 mmHg as pPRA, suggesting that the circumferential recoiling must be lower for the hPRA compared with the pPRA (similar to the lack of longitudinal recoiling upon excision). These findings are supported by mathematical modeling of the stress-strain relationships showing that collagen is engaged at significantly lower strains in hPRA than in pPRA. Furthermore, the elastic modulus of the elastin component of the hPRA arterial wall was significantly lower than that of pPRA, whereas that of collagen was significantly higher. Vital imaging, including quantitative measurements of the microarchitecture of the adventitial collagen and the IEL, supports that the microarchitecture of collagen in the hPRA, being almost straight at low transmural pressure and strain, restrains the geometry of the hPRA significantly.

Combined imaging and mechanical studies have supported the development of microstructurally motivated mathematical models of the arterial wall. However, the majority of these studies were conducted on large, elastic conduit arteries (15, 16, 28, 58, 71). A recent paper (6) has opened the discussion of the mechanobiology of vascular

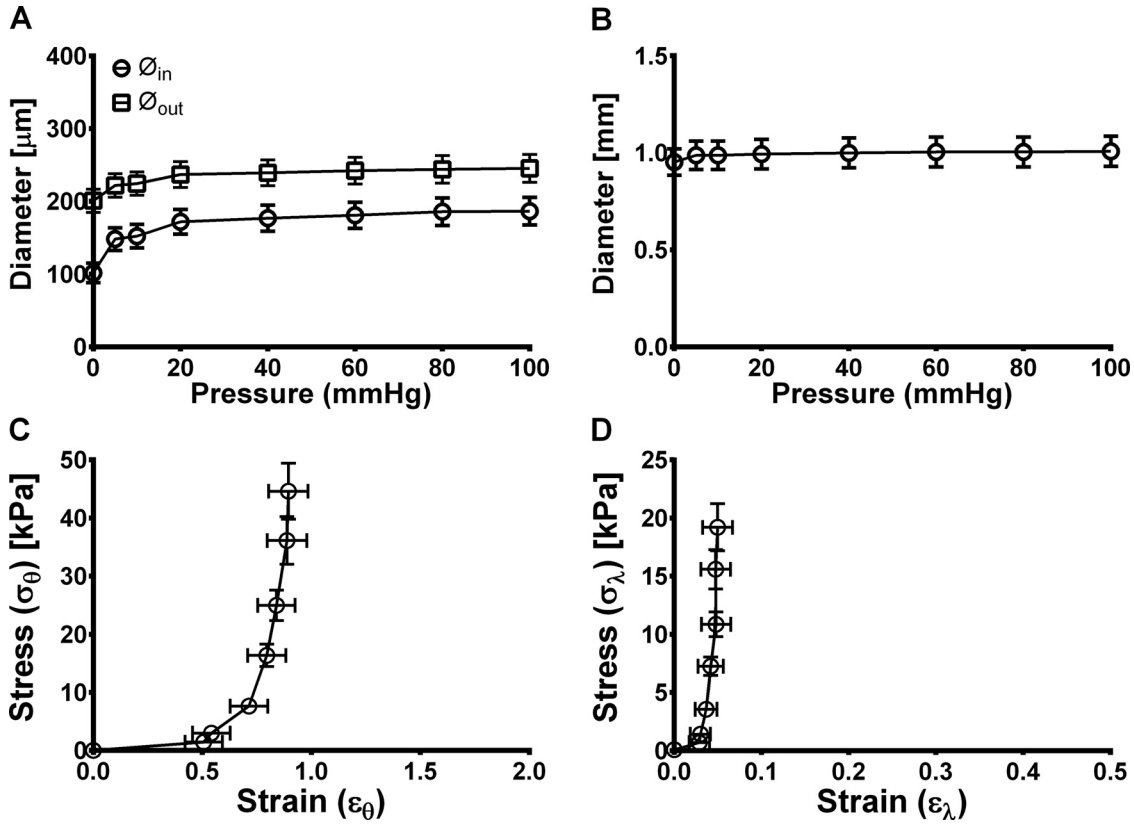

Fig. 7. Structural and mechanical characteristics of human pericardial resistance arteries (hPRAs) as a function of increasing transmural pressure. *A*: pressure-diameter, *B*: pressure-length, *C*: circumferential stress-strain, and *D*: longitudinal stress-strain relationships from 12 individual patients' pericardial resistance arteries. The layout of this figure was intentionally designed similar to that of Fig. 1 for comparison.

remodeling in human resistance arteries, addressing the pressure-induced reorganization of the IEL and adventitial collagen, including a multilayer analytical model to calculate the stiffness and stress in each layer of the arterial wall. In that study (6), hSCAs were obtained from healthy volunteers, and the arteries were studied between 0 and 50 mmHg, with structures and related stresses reported for 3 and 30 mmHg, respectively. Our study illustrates the potential of applying imaging and biomechanical testing integrated with constitutive mathematical modeling to improve understanding of the relationships between arterial wall mechanics and the microarchitecture of the ECM in healthy and diseased resistance arteries. Although simple compared with other mathematical models, taking into account also the spatial distribution of collagen and elastin fibers (7, 28, 69), the applied mathematical model provides useful insights in the structure and function of resistance arteries. Importantly, we provide evidence that in the PRA from patients with cardiovascular disease, collagen constrains axial as well as radial changes in structure with increasing pressure. In particular, it was a surprise that the hPRA axially showed such a large variation in deformation, with half of the investigated arteries not changing length at all upon pressurization (0−100 mmHg). Whether this is a consequence of aging or the presence of cardiovascular disease remains to be investigated.

The PRA resides in the parietal pericardium, a fibrous tissue rich in collagen with only a few elastin fibers (9). The role of the pericardium is to support the heart and prevent it from overstretching during diastole (37). Both pig and human PRAs show a sparse but distinct EEL and an IEL comprising longitudinally aligned elastin fibers interconnected with thinner fibers (9). The pPRA EEL visually appears structurally similar to that of the EEL in rat cremaster arteries (17). Previous studies have shown that arteries residing in tissues subject to longitudinal stretches show a distinct EEL, recoil significantly upon excision, and lengthen considerably (35%) upon elastase digestion while the pressure-diameter curve is left shifted at lower pressures after elastase treatment (17). Treatment of these arteries with collagenase, on the other hand, did not affect their length but shifted the pressure-diameter curve upward (17). Other studies in rMA have reported considerable effects of elastase treatment on diameter and stiffness (12, 30), accomplished by a significant decrease in adventitial elastin fiber content and increased IEL fenestrae area (12, 30). In contrast, rat cerebral arteries, protected from longitudinal stretching due to the brain being protected by the skull, show no EEL and no lengthening upon elastase treatment (17). In the pPRA, we confirmed a role for elastin in bearing longitudinal stress (17). The concentrations of enzymes used in our study were titrated to keep the individual arteries from leaking and to remain contractile. The lengthening of the pPRA upon elastase treatment was not as pronounced, as reported for rat cremaster arteries (17), and the considerable upward shift in the pressure-diameter curve of collagenase-treated arteries was much larger than reported for rat cremaster and mesenteric arteries (12, 17,

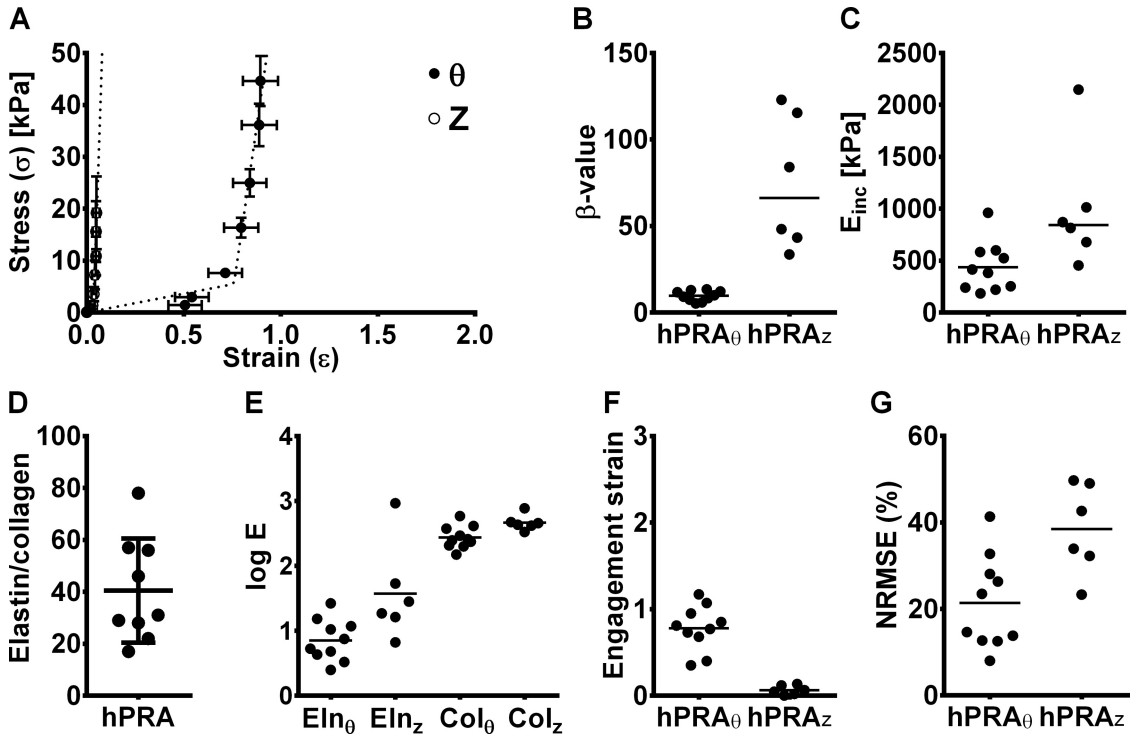

Fig. 8. Parameter estimates from fitting the stress-strain relationships and mathematical modeling of the hPRA. *A*: stress-strain relationship with the mathematical model (dotted lines) superimposed on the original data points [circumference (θ): ●; longitude (*z*): ○]. *B* and *C*: individual β-values (*B*) and calculated E_{inc} (*C*) at a transmural pressure of 100 mmHg. *D*: elastin-to-collagen volume ratios calculated from imaging data. *E*: elastin (Eln) and collagen (Col) stiffness in the circumferential and longitudinal directions, respectively. *F*: collagen recruitment strain, estimated from the mathematical model. *G*: NRMSE, a measure of the errors between measured wall stress and model-predicted wall stress. The layout of this figure was intentionally designed similar to that of Fig. 4 for comparison.

30). Our findings are in line with previous reports stating a dominant role of elastin primarily at lower pressures while the wall stress increasingly is borne by the more rigid collagen at higher pressures and wall strains (21, 32, 38, 66, 67), also referred to as the progressive "hook on" or recruitment of collagen fibers (3, 66). Whether the arteries in the pericardium are subject to longitudinal stretching within the tissue remains to be elucidated. Clinically, the parietal pericardium appears rigid (37), an observation supported by its collagenous composition.

The hPRA in our study showed very small circumferential distensibility and elongation. We compared lumen diameters, wall thicknesses, wall cross-sectional area, and wall-to-lumen ratios at 100 mmHg to previously reported findings in hSCAs. These vessels are frequently used for studies of human resistance artery remodeling (14, 18–20, 33, 39, 42, 44, 57). Importantly, our observations on geometry, as well as the β-values, proportional to E_{inc}, are within the range of previously published observations in hSCAs studied under similar conditions (33, 39, 57). This supports that the hPRA is a valuable addition for clinically relevant investigations of the reactivity and the mechanobiology of the human microcirculation from aged, diseased patients.

The most important finding in our study is that acute pressure-induced structural changes of the hPRA are small, strongly supported by imaging data and mathematical modeling, suggesting that the microarchitecture (straightness) and increased stiffness of collagen are the limiting factors. It has previously been shown in the pig thoracic aorta that elevated stiffness is observed consistently for regions with sharper and earlier collagen recruitment and less undulation in collagen fibers (71). Recent studies have shown by means of constitutive modeling of in vivo ultrasound pressure-area data on human carotid arteries an age-related shift in pressure-load bearing from elastin to collagen, caused by a decrease in elastin stiffness and a considerable increase in collagen recruitment in human carotid arteries (49, 62). Furthermore, as recently suggested by Gautieri et al. (29), nonenzymatic glycation of collagen reduces tissue viscoelasticity by severely limiting collagen fiber-fiber and fibril-fibril sliding. The molecular nature of the arterial wall explaining the observed recruitment of collagen already at low transmural pressure and strain as well as the lack of change in the microarchitecture with pressure in the hPRA remains to be determined. It is generally accepted that essential hypertension, diabetes, and the metabolic syndrome are associated with significant remodeling of the arterial wall, including compositional changes of the ECM (11, 35, 52, 54, 65). Our use of arteries from patients undergoing cardiothoracic surgeries allows investigations in vessels from individuals of different sex, disease history (e.g., diabetes), pharmacological treatments, and age. However, deciphering the influences of each of these variables requires a large number of patients and their arteries, comparisons between randomized groups, and multifactorial analyses.

Future extension of the integrated approach. In our study, we focused on the passive mechanical properties of the arterial wall, considering only the ECM as a key element. However, not only the quantity but also the quality, integrity, and structural organi-

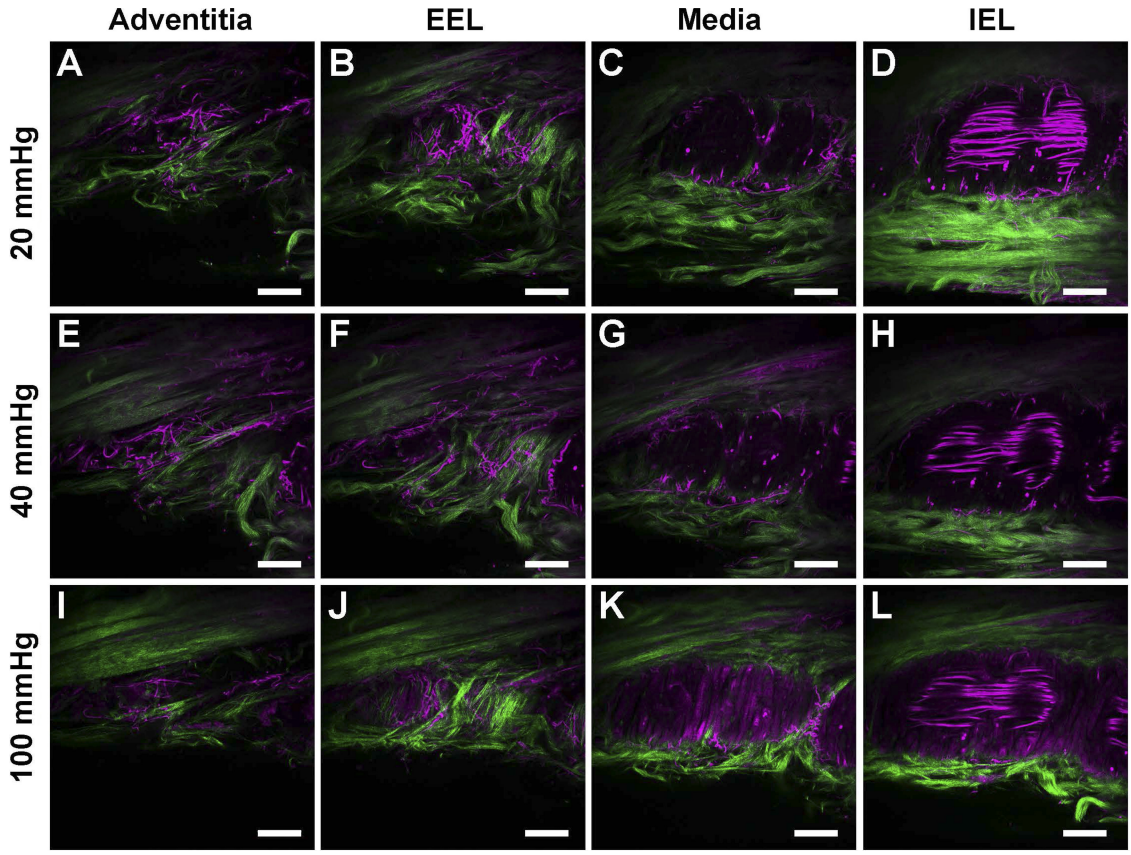

Fig. 9. Microarchitecture of the extracellular matrix of a hPRA as a function of increasing pressure. Two-photon excitation fluorescence microscopy images of collagen (green) and elastin (magenta) at 20 mmHg (*A–D*), 40 mmHg (*E–H*), and 100 mmHg (*I–L*) in the tunica adventitia (*A*, *E*, and *I*), EEL (*B*, *F*, and *J*), tunica media (*C*, *G*, and *K*), and IEL (*D*, *H*, and *L*) are shown. The image series is representative of three independent experiments. Scale bars = 10 μm.

zation and interaction of the different constituents of the ECM, including live cells, have an impact on the stiffness of the arterial wall (8, 12, 27, 28, 30, 68). Recent evidence suggests that the stiffness of SMCs should also be taken into account (59, 60). Furthermore, the relationship between the arterial mechanics and vasomotor tone should be addressed through studies of mechanotransduction, the response of the arteries to increased shear and wall stresses. Before doing so, an active SMC component must be added to the mathematical model, and its contribution to the biaxial mechanics must be verified (63). Finally, not only the orientation and distribution of SMC but also the orientation and distribution of endothelial cells may be a qualified addition (45).

Conclusions. To the best of our knowledge, this report is the first to demonstrate the integrated use of imaging, biomechanical testing, and mathematical modeling to improve our understanding of the relationship between the arterial wall mechanics and microarchitecture of the ECM in resistance arteries from an animal model translated to the diseased human microvasculature.

Our integrated approach invites detailed and integrative studies of the relationship between the microarchitecture of the

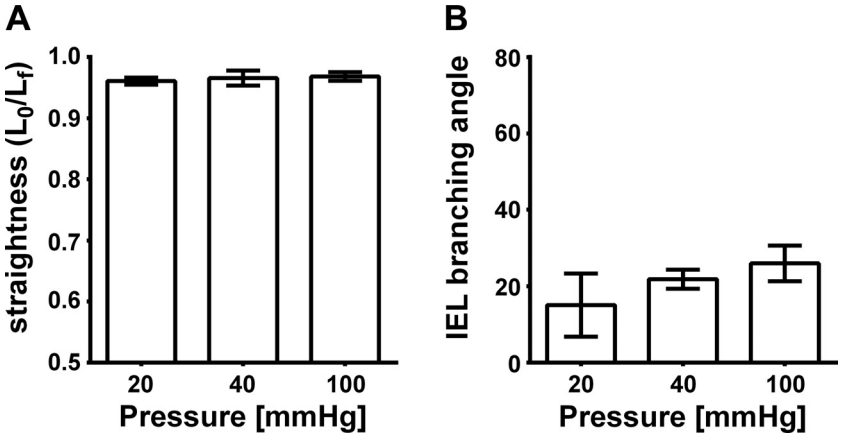

Fig. 10. Microstructural changes in adventitial collagen and the IEL in hPRAs are limited. *A*: straightness L_0/L_f [collagen fiber bundle end-to-end length via a straight line (L_0)/full length (L_f)] of collagen fibers present at the border between the EEL and tunica adventitia. *B*: branching angles for elastin fibers in the IEL, each determined for three individual arteries (at 20 mmHg, $n = 2$).

ECM and remodeling of resistance arteries to improve our understanding of the mechanobiology of the microcirculation in aging and cardiovascular disease.

ACKNOWLEDGMENTS

We are grateful to the patients for providing their tissue for research. We thank Pia Søndergaard Jensen (Odense University Hospital Elite Research Centre for Individualized Medicine in Arterial Diseases) for her assistance in collecting patient informed consent forms and biopsies. Skallebølle and Vester Hæsinge Slaughterhouses are acknowledged for the supply of pig pericardial tissues, and the Danish Molecular BioImaging Center is acknowledged for the use of equipment. Prof. Paul M. Vanhoutte (University of Hong Kong) is acknowledged for critical reading and valuable feedback on the manuscript.

Present addresses: B. Spronck, Dept. of Biomedical Sciences, Faculty of Medicine and Heath Sciences, Macquarie Univ., 75 Talavera Rd., Level 1, Macquarie Park, NSW 2113, Australia.

Present address of L. A. Bagatolli: Yachay EP and Yachay Tech, 100651 Yachay City of Knowledge, Ecuador.

GRANTS

This work was conducted within the framework of the Odense University Hospital Elite Research Center, Centre for Individualized Medicine in Arterial Diseases, and was supported by the Odense University Hospital and University of Southern Denmark. M. H. G. Heusinkveld was supported by a Kootstra Talent Fellowship by the Maastricht University Medical Center. B. Spronck was supported by an Endeavor Research Fellowship awarded by the Australian Government.

DISCLOSURES

No conflicts of interest, financial or otherwise, are declared by the authors.

AUTHOR CONTRIBUTIONS

M.B., T.M.L., B.S., M.H.H., J.R.B., L.A.B., K.D.R., and J.G.D.M. conceived and designed research; M.B., B.S., M.H.H., K.R., I.N., U.M.H., and K.D.R. performed experiments; M.B., B.S., M.H.H., B.T., K.R., I.N., U.M.H., J.R.B., K.D.R., and J.G.D.M. analyzed data; M.B., T.M.L., B.S., M.H.H., B.T., K.R., I.N., J.R.B., L.A.B., L.M.R., A.I., K.D.R., and J.G.D.M. interpreted results of experiments; M.B. prepared figures; M.B. and J.G.D.M. drafted manuscript; M.B., T.M.L., B.S., M.H.H., B.T., K.R., I.N., U.M.H., J.R.B., L.A.B., L.M.R., A.I., K.D.R., and J.G.D.M. edited and revised manuscript; M.B., T.M.L., B.S., M.H.H., B.T., K.R., I.N., U.M.H., J.R.B., L.A.B., L.M.R., A.I., K.D.R., and J.G.D.M. approved final version of manuscript.

REFERENCES

1. **Arribas SM, Hillier C, González C, McGrory S, Dominiczak AF, McGrath JC.** Cellular aspects of vascular remodeling in hypertension revealed by confocal microscopy. *Hypertension* 30: 1455–1464, 1997. doi:10.1161/01.HYP.30.6.1455.
2. **Arribas SM, Hinek A, González MC.** Elastic fibres and vascular structure in hypertension. *Pharmacol Ther* 111: 771–791, 2006. doi:10.1016/j.pharmthera.2005.12.003.
3. **Bakker EN, Groma G, Spijkers LJ, de Vos J, van Weert A, van Veen H, Everts V, Arribas SM, VanBavel E.** Heterogeneity in arterial remodeling among sublines of spontaneously hypertensive rats. *PLoS One* 9: e107998, 2014. doi:10.1371/journal.pone.0107998.
4. **Bakker EN, Pistea A, Spaan JA, Rolf T, de Vries CJ, van Rooijen N, Candi E, VanBavel E.** Flow-dependent remodeling of small arteries in mice deficient for tissue-type transglutaminase: possible compensation by macrophage-derived factor XIII. *Circ Res* 99: 86–92, 2006. doi:10.1161/01.RES.0000229657.83816.a7.
5. **Bakker EN, Pistea A, VanBavel E.** Transglutaminases in vascular biology: relevance for vascular remodeling and atherosclerosis. *J Vasc Res* 45: 271–278, 2008. doi:10.1159/000113599.
6. **Bell JS, Adio AO, Pitt A, Hayman L, Thorn CE, Shore AC, Whatmore JL, Winlove CP.** Microstructure and mechanics of human resistance arteries. *Am J Physiol Heart Circ Physiol* 311: H1560–H1568, 2016. doi:10.1152/ajpheart.00002.2016.
7. **Bellini C, Ferruzzi J, Roccabianca S, Di Martino ES, Humphrey JD.** A microstructurally motivated model of arterial wall mechanics with mechanobiological implications. *Ann Biomed Eng* 42: 488–502, 2014. doi:10.1007/s10439-013-0928-x.
8. **Bersi MR, Ferruzzi J, Eberth JF, Gleason RL Jr, Humphrey JD.** Consistent biomechanical phenotyping of common carotid arteries from seven genetic, pharmacological, and surgical mouse models. *Ann Biomed Eng* 42: 1207–1223, 2014. doi:10.1007/s10439-014-0988-6.
9. **Bloksgaard M, Leurgans TM, Nissen I, Jensen PS, Hansen ML, Brewer JR, Bagatolli LA, Marcussen N, Irmukhamedov A, Rasmussen LM, De Mey JGR.** Elastin organization in pig and cardiovascular disease patients' pericardial resistance arteries. *J Vasc Res* 52: 1–11, 2015. doi:10.1159/000376548.
10. **Brewer J, Bloksgaard M, Kubiak J, Sørensen JA, Bagatolli LA.** Spatially resolved two-color diffusion measurements in human skin applied to transdermal liposome penetration. *J Invest Dermatol* 133: 1260–1268, 2013. doi:10.1038/jid.2012.461.
11. **Briones AM, Arribas SM, Salaices M.** Role of extracellular matrix in vascular remodeling of hypertension. *Curr Opin Nephrol Hypertens* 19: 187–194, 2010. doi:10.1097/MNH.0b013e328335eec9.
12. **Briones AM, González JM, Somoza B, Giraldo J, Daly CJ, Vila E, González MC, McGrath JC, Arribas SM.** Role of elastin in spontaneously hypertensive rat small mesenteric artery remodelling. *J Physiol* 552: 185–195, 2003. doi:10.1113/jphysiol.2003.046904.
13. **Briones AM, Xavier FE, Arribas SM, González MC, Rossoni LV, Alonso MJ, Salaices M.** Alterations in structure and mechanics of resistance arteries from ouabain-induced hypertensive rats. *Am J Physiol Heart Circ Physiol* 291: H193–H201, 2006. doi:10.1152/ajpheart.00802.2005.
14. **Buus NH, Mathiassen ON, Fenger-Grøn M, Præstholm MN, Sihm I, Thybo NK, Schroeder AP, Thygesen K, Aalkjær C, Pedersen OL, Mulvany MJ, Christensen KL.** Small artery structure during antihypertensive therapy is an independent predictor of cardiovascular events in essential hypertension. *J Hypertens* 31: 791–797, 2013. doi:10.1097/HJH.0b013e32835e215e.
15. **Chen H, Slipchenko MN, Liu Y, Zhao X, Cheng JX, Lanir Y, Kassab GS.** Biaxial deformation of collagen and elastin fibers in coronary adventitia. *J Appl Physiol (1985)* 115: 1683–1693, 2013. doi:10.1152/japplphysiol.00601.2013.
16. **Chow MJ, Turcotte R, Lin CP, Zhang Y.** Arterial extracellular matrix: a mechanobiological study of the contributions and interactions of elastin and collagen. *Biophys J* 106: 2684–2692, 2014. doi:10.1016/j.bpj.2014.05.014.
17. **Clifford PS, Ella SR, Stupica AJ, Nourian Z, Li M, Martinez-Lemus LA, Dora KA, Yang Y, Davis MJ, Pohl U, Meininger GA, Hill MA.** Spatial distribution and mechanical function of elastin in resistance arteries: a role in bearing longitudinal stress. *Arterioscler Thromb Vasc Biol* 31: 2889–2896, 2011. doi:10.1161/ATVBAHA.111.236570.
18. **De Ciuceis C, Porteri E, Rizzoni D, Corbellini C, La Boria E, Boari GE, Pilu A, Mittempergher F, Di Betta E, Casella C, Nascimbeni R, Rosei CA, Ruggeri G, Caimi L, Rosei EA.** Effects of weight loss on structural and functional alterations of subcutaneous small arteries in obese patients. *Hypertension* 58: 29–36, 2011. doi:10.1161/HYPERTENSIONAHA.111.171082.
19. **De Ciuceis C, Porteri E, Rizzoni D, Rizzardi N, Paiardi S, Boari GE, Miclini M, Zani F, Muiesan ML, Donato F, Salvetti M, Castellano M, Tiberio GA, Giulini SM, Agabiti Rosei E.** Structural alterations of subcutaneous small-resistance arteries may predict major cardiovascular events in patients with hypertension. *Am J Hypertens* 20: 846–852, 2007. doi:10.1016/j.amjhyper.2007.03.016.
20. **De Ciuceis C, Savoia C, Arrabito E, Porteri E, Mazza M, Rossini C, Duse S, Semeraro F, Agabiti Rosei C, Alonzo A, Sada L, La Boria E, Sarkar A, Petroboni B, Mercantini P, Volpe M, Rizzoni D, Agabiti Rosei E.** Effects of a long-term treatment with aliskiren or ramipril on structural alterations of subcutaneous small-resistance arteries of diabetic hypertensive patients. *Hypertension* 64: 717–724, 2014. doi:10.1161/HYPERTENSIONAHA.114.03380.
21. **Dobrin PB.** Mechanical properties of arteries. *Physiol Rev* 58: 397–460, 1978.
22. **Drummond GB, Paterson DJ, McLoughlin P, McGrath JC.** Statistics: all together now, one step at a time. *Adv Physiol Educ* 35: 129, 2011. doi:10.1152/advan.00029.2011.
23. **Drummond GB, Tom BD.** Presenting data: can you follow a recipe? *Br J Pharmacol* 165: 777–781, 2012. doi:10.1111/j.1476-5381.2011.01735.x.
24. **Drummond GB, Tom BD.** Statistics, probability, significance, likelihood: words mean what we define them to mean. *Adv Physiol Educ* 35: 361–364, 2011. doi:10.1152/advan.00060.2011.

25. **Drummond GB, Vowler SL.** Do as you would be done by: write as you would wish to read. *J Physiol* 590: 6251–6254, 2012. doi:10.1113/jphysiol.2012.248278.
26. **Drummond GB, Vowler SL.** Not different is not the same as the same: how can we tell? *Clin Exp Pharmacol Physiol* 39: 991–994, 2012. doi:10.1111/1440-1681.12008.
27. **Ferruzzi J, Bersi MR, Uman S, Yanagisawa H, Humphrey JD.** Decreased elastic energy storage, not increased material stiffness, characterizes central artery dysfunction in fibulin-5 deficiency independent of sex. *J Biomech Eng* 137: 031007, 2015. doi:10.1115/1.4029431.
28. **Fonck E, Prod'hom G, Roy S, Augsburger L, Rüfenacht DA, Stergiopulos N.** Effect of elastin degradation on carotid wall mechanics as assessed by a constituent-based biomechanical model. *Am J Physiol Heart Circ Physiol* 292: H2754–H2763, 2007. doi:10.1152/ajpheart.01108.2006.
29. **Gautieri A, Passini FS, Silvan U, Guizar-Sicairos M, Carimati G, Volpi P, Moretti M, Schoenhuber H, Redaelli A, Berli M, Snedeker JG.** Advanced glycation end-products: mechanics of aged collagen from molecule to tissue. *Matrix Biol* 59: 95−108, 2017. doi:10.1016/j.matbio.2016.09.001.
30. **González JM, Briones AM, Somoza B, Daly CJ, Vila E, Starcher B, McGrath JC, González MC, Arribas SM.** Postnatal alterations in elastic fiber organization precede resistance artery narrowing in SHR. *Am J Physiol Heart Circ Physiol* 291: H804–H812, 2006. doi:10.1152/ajpheart.01262.2005.
31. **González JM, Briones AM, Starcher B, Conde MV, Somoza B, Daly C, Vila E, McGrath I, González MC, Arribas SM.** Influence of elastin on rat small artery mechanical properties. *Exp Physiol* 90: 463–468, 2005. doi:10.1113/expphysiol.2005.030056.
32. **Green EM, Mansfield JC, Bell JS, Winlove CP.** The structure and micromechanics of elastic tissue. *Interface Focus* 4: 20130058, 2014. doi:10.1098/rsfs.2013.0058.
33. **Greenstein AS, Price A, Sonoyama K, Paisley A, Khavandi K, Withers S, Shaw L, Paniagua O, Malik RA, Heagerty AM.** Eutrophic remodeling of small arteries in type 1 diabetes mellitus is enabled by metabolic control: a 10-year follow-up study. *Hypertension* 54: 134–141, 2009. doi:10.1161/HYPERTENSIONAHA.109.129718.
34. **Guo H, Humphrey JD, Davis MJ.** Effects of biaxial stretch on arteriolar function in vitro. *Am J Physiol Heart Circ Physiol* 292: H2378–H2386, 2007. doi:10.1152/ajpheart.00810.2006.
35. **Heagerty AM, Heerkens EH, Izzard AS.** Small artery structure and function in hypertension. *J Cell Mol Med* 14: 1037–1043, 2010. doi:10.1111/j.1582-4934.2010.01080.x.
36. **Hilgers RH, Bergaya S, Schiffers PM, Meneton P, Boulanger CM, Henrion D, Lévy BI, De Mey JG.** Uterine artery structural and functional changes during pregnancy in tissue kallikrein-deficient mice. *Arterioscler Thromb Vasc Biol* 23: 1826–1832, 2003. doi:10.1161/01.ATV.0000090672.07568.60.
37. **Holt JP.** The normal pericardium. *Am J Cardiol* 26: 455–465, 1970. doi:10.1016/0002-9149(70)90702-2.
38. **Humphrey JD, Dufresne ER, Schwartz MA.** Mechanotransduction and extracellular matrix homeostasis. *Nat Rev Mol Cell Biol* 15: 802–812, 2014. doi:10.1038/nrm3896.
39. **Intengan HD, Deng LY, Li JS, Schiffrin EL.** Mechanics and composition of human subcutaneous resistance arteries in essential hypertension. *Hypertension* 33: 569–574, 1999. doi:10.1161/01.HYP.33.1.569.
40. **Intengan HD, Schiffrin EL.** Structure and mechanical properties of resistance arteries in hypertension: role of adhesion molecules and extracellular matrix determinants. *Hypertension* 36: 312–318, 2000. doi:10.1161/01.HYP.36.3.312.
41. **Intengan HD, Thibault G, Li JS, Schiffrin EL.** Resistance artery mechanics, structure, and extracellular components in spontaneously hypertensive rats: effects of angiotensin receptor antagonism and converting enzyme inhibition. *Circulation* 100: 2267–2275, 1999. doi:10.1161/01.CIR.100.22.2267.
42. **Lynch FM, Izzard AS, Austin C, Prendergast B, Keenan D, Malik RA, Heagerty AM.** Effects of diabetes and hypertension on structure and distensibilty of human small coronary arteries. *J Hypertens* 30: 384–389, 2012. doi:10.1097/HJH.0b013e32834e38a0.
43. **Martinez-Lemus LA, Hill MA, Meininger GA.** The plastic nature of the vascular wall: a continuum of remodeling events contributing to control of arteriolar diameter and structure. *Physiology (Bethesda)* 24: 45–57, 2009. doi:10.1152/physiol.00029.2008.
44. **Mathiassen ON, Buus NH, Sihm I, Thybo NK, Mørn B, Schroeder AP, Thygesen K, Aalkjaer C, Lederballe O, Mulvany MJ, Christensen KL.** Small artery structure is an independent predictor of cardiovascular events in essential hypertension. *J Hypertens* 25: 1021–1026, 2007. doi:10.1097/HJH.0b013e32805bf8ed.
45. **McGrath JC, Deighan C, Briones AM, Shafaroudi MM, McBride M, Adler J, Arribas SM, Vila E, Daly CJ.** New aspects of vascular remodelling: the involvement of all vascular cell types. *Exp Physiol* 90: 469–475, 2005. doi:10.1113/expphysiol.2005.030130.
46. **Meijering E, Jacob M, Sarria JC, Steiner P, Hirling H, Unser M.** Design and validation of a tool for neurite tracing and analysis in fluorescence microscopy images. *Cytometry A* 58: 167–176, 2004. doi:10.1002/cyto.a.20022.
47. **Mulvany MJ.** Resistance vessel growth and remodelling: cause or consequence in cardiovascular disease. *J Hum Hypertens* 9: 479–485, 1995.
48. **Mulvany MJ.** Small artery remodelling in hypertension. *Basic Clin Pharmacol Toxicol* 110: 49–55, 2012. doi:10.1111/j.1742-7843.2011.00758.x.
49. **O'Rourke MF, Hashimoto J.** Mechanical factors in arterial aging: a clinical perspective. *J Am Coll Cardiol* 50: 1–13, 2007. doi:10.1016/j.jacc.2006.12.050.
50. **Pourageaud F, Crabos M, Freslon JL.** The elastic modulus of conductance coronary arteries from spontaneously hypertensive rats is increased. *J Hypertens* 15: 1113–1121, 1997. doi:10.1097/00004872-199715100-00009.
51. **Rezakhaniha R, Agianniotis A, Schrauwen JT, Griffa A, Sage D, Bouten CV, van de Vosse FN, Unser M, Stergiopulos N.** Experimental investigation of collagen waviness and orientation in the arterial adventitia using confocal laser scanning microscopy. *Biomech Model Mechanobiol* 11: 461–473, 2012. doi:10.1007/s10237-011-0325-z.
52. **Rizzoni D, Agabiti-Rosei E.** Structural abnormalities of small resistance arteries in essential hypertension. *Intern Emerg Med* 7: 205–212, 2012. doi:10.1007/s11739-011-0548-0.
53. **Sandow SL, Gzik DJ, Lee RM.** Arterial internal elastic lamina holes: relationship to function? *J Anat* 214: 258–266, 2009. doi:10.1111/j.1469-7580.2008.01020.x.
54. **Schiffrin EL.** Vascular remodeling in hypertension: mechanisms and treatment. *Hypertension* 59: 367–374, 2012. doi:10.1161/HYPERTENSIONAHA.111.187021.
55. **Schiffrin EL, Hayoz D.** How to assess vascular remodelling in small and medium-sized muscular arteries in humans. *J Hypertens* 15: 571–584, 1997. doi:10.1097/00004872-199715060-00002.
56. **Schindelin J, Arganda-Carreras I, Frise E, Kaynig V, Longair M, Pietzsch T, Preibisch S, Rueden C, Saalfeld S, Schmid B, Tinevez JY, White DJ, Hartenstein V, Eliceiri K, Tomancak P, Cardona A.** Fiji: an open-source platform for biological-image analysis. *Nat Methods* 9: 676–682, 2012. doi:10.1038/nmeth.2019.
57. **Schofield I, Malik R, Izzard A, Austin C, Heagerty A.** Vascular structural and functional changes in type 2 diabetes mellitus: evidence for the roles of abnormal myogenic responsiveness and dyslipidemia. *Circulation* 106: 3037–3043, 2002. doi:10.1161/01.CIR.0000041432.80615.A5.
58. **Schriefl AJ, Schmidt T, Balzani D, Sommer G, Holzapfel GA.** Selective enzymatic removal of elastin and collagen from human abdominal aortas: uniaxial mechanical response and constitutive modeling. *Acta Biomater* 17: 125–136, 2015. doi:10.1016/j.actbio.2015.01.003.
59. **Sehgel NL, Sun Z, Hong Z, Hunter WC, Hill MA, Vatner DE, Vatner SF, Meininger GA.** Augmented vascular smooth muscle cell stiffness and adhesion when hypertension is superimposed on aging. *Hypertension* 65: 370–377, 2015. doi:10.1161/HYPERTENSIONAHA.114.04456.
60. **Sehgel NL, Vatner SF, Meininger GA.** "Smooth muscle cell stiffness syndrome"-revisiting the structural basis of arterial stiffness. *Front Physiol* 6: 335, 2015. doi:10.3389/fphys.2015.00335.
61. **Sommer C, Straehle C, Kothe U, Hamprecht FA.** Ilastik: Interactive Learning and Segmentation Toolkit. *IEEE International Symposium on Biomedical Imaging* Chicago, IL: March 30−April 2, 2011. p. 230–233.
62. **Spronck B, Heusinkveld MH, Donders WP, de Lepper AG, Op't Roodt J, Kroon AA, Delhaas T, Reesink KD.** A constitutive modeling interpretation of the relationship among carotid artery stiffness, blood pressure, and age in hypertensive subjects. *Am J Physiol Heart Circ Physiol* 308: H568–H582, 2015. doi:10.1152/ajpheart.00290.2014.
63. **Spronck B, Megens RT, Reesink KD, Delhaas T.** A method for three-dimensional quantification of vascular smooth muscle orientation: application in viable murine carotid arteries. *Biomech Model Mechanobiol* 15: 419–432, 2016. doi:10.1007/s10237-015-0699-4.

64. **Staiculescu MC, Galiñanes EL, Zhao G, Ulloa U, Jin M, Beig MI, Meininger GA, Martinez-Lemus LA.** Prolonged vasoconstriction of resistance arteries involves vascular smooth muscle actin polymerization leading to inward remodelling. *Cardiovasc Res* 98: 428–436, 2013. doi:10.1093/cvr/cvt034.
65. **van den Akker J, Schoorl MJ, Bakker EN, Vanbavel E.** Small artery remodeling: current concepts and questions. *J Vasc Res* 47: 183–202, 2010. doi:10.1159/000255962.
66. **VanBavel E, Siersma P, Spaan JA.** Elasticity of passive blood vessels: a new concept. *Am J Physiol Heart Circ Physiol* 285: H1986–H2000, 2003. doi:10.1152/ajpheart.00248.2003.
67. **Wagenseil JE, Mecham RP.** Vascular extracellular matrix and arterial mechanics. *Physiol Rev* 89: 957–989, 2009. doi:10.1152/physrev.00041.2008.
68. **Wagenseil JE, Nerurkar NL, Knutsen RH, Okamoto RJ, Li DY, Mecham RP.** Effects of elastin haploinsufficiency on the mechanical behavior of mouse arteries. *Am J Physiol Heart Circ Physiol* 289: H1209–H1217, 2005. doi:10.1152/ajpheart.00046.2005.
69. **Weisbecker H, Unterberger MJ, Holzapfel GA.** Constitutive modelling of arteries considering fibre recruitment and three-dimensional fibre distribution. *J R Soc Interface* 12: 20150111, 2015. doi:10.1098/rsif.2015.0111.
70. **World Medical Association.** World Medical Association Declaration of Helsinki: ethical principles for medical research involving human subjects. *JAMA* 310: 2191–2194, 2013. doi:10.1001/jama.2013.281053.
71. **Zeinali-Davarani S, Wang Y, Chow MJ, Turcotte R, Zhang Y.** Contribution of collagen fiber undulation to regional biomechanical properties along porcine thoracic aorta. *J Biomech Eng* 137: 051001, 2015. doi:10.1115/1.4029637.